Remote Sensing of Environment 146 (2014) 77–86

Contents lists available at ScienceDirect

Remote Sensing of Environment

journal homepage: www.elsevier.com/locate/rse

Enhancement of primary production in the North Atlantic outside of the spring bloom, identified by remote sensing of ocean colour and temperature

Gavin H. Tilstone [a,*], Peter I. Miller [a], Robert J.W. Brewin [a], Imants G. Priede [b]

[a] Plymouth Marine Laboratory, Prospect Place, West Hoe, Plymouth PL1 3DH, UK
[b] Oceanlab, University of Aberdeen, Main Street, Newburgh, Aberdeen AB41 6AA, UK

ARTICLE INFO

Article history:
Received 7 October 2012
Received in revised form 12 March 2013
Accepted 5 April 2013
Available online 4 October 2013

Keywords:
Phytoplankton
Primary production
North Atlantic
Reykjanes Ridge
Sub-polar front
Sea surface temperature

ABSTRACT

The heterogeneity in phytoplankton production in the North Atlantic after the spring bloom is poorly understood. We analysed merged microwave and infrared satellite sea surface temperature (SST) data and ocean colour phytoplankton size class biomass, primary production (PP) and new production (ExP) derived from SeaWiFS data, to assess the spatial and temporal frequency of surface thermal fronts and areas of enhanced PP and ExP. Strong and persistent surface thermal fronts occurred at the Reykjanes Ridge (RR) and sub-polar front (SPF), which sustain high PP and ExP and, outside of the spring bloom, account for 9% and 15% of the total production in the North Atlantic. When normalised by area, PP at the SPF is four times higher than the RR. Analysis of 13 years of satellite ocean colour data from SeaWiFS, and compared with MODIS-Aqua and MERIS, showed that there was no increase in Chla from 1998 to 2002, which then decreased in all areas from 2002 to 2007 and was most pronounced in the RR. These time series also illustrated that the SPF exhibited the highest PP and the lowest variation in Chla over the ocean colour record. This implies that the SPF provides a high and consistent supply of carbon to the benthos irrespective of fluctuations in the North Atlantic Oscillation.

1. Introduction

Phytoplankton are responsible for about half of the global primary production (PP) (Longhurst, Sathyendranath, Platt, & Caverhill, 1995) and in the North Atlantic, represent a significant sink for carbon dioxide (Takahashi et al., 2009). North Atlantic sub-polar waters account for ~50% of the global ocean productivity and >80% of the organic flux to the sea floor (Wassmann, 1990). The principal signal is from the spring bloom, which evolves northwards from April to June as the winter mixed-layer shoals, exposing high nutrient concentrations in the surface layers to light as incident irradiance and day length increase (Sverdrup, 1957). The magnitude of the spring bloom in this region is one of the largest in the global ocean and is controlled by a combination of physical forcing and biological factors (Koertzinger et al., 2008), with its timing driven strongly by physical forcing (Henson, Dunne, & Sarmiento, 2009). After the spring bloom, PP becomes patchy, both in space and time, and this heterogeneity is poorly understood (Dutkiewicz, Follows, Marshall, & Gregg, 2001).

Frontal systems have long been recognised as areas of high phytoplankton biomass and PP (Pingree, Kuo, & Garcia-Soto, 2002). Increases in biomass have been observed along the cyclonic side of the Gulf Stream (Hitchcock, Langdon, & Smayda, 1987). Ocean fronts around the Grand Banks in the North Atlantic are associated with high phytoplankton biomass, which is sustained by an inhibition of turbulent mixing through frontal re-stratification (Taylor & Ferrari, 2011). Enhanced vertical mixing is a common feature over the Mid-Atlantic Ridge (MAR), which can cause anomalies in salinity, oxygen and nutrients (Mauritzen, Polzin, McCartney, Millard, & West-Mack, 2002). We used a combination of microwave, infrared SST and ocean colour data to assess the frequency of surface thermal fronts and associated PP and ExP in the North Atlantic. We tested the hypothesis; are the Reykjanes Ridge and sub-polar front areas of high PP and ExP outside of the spring bloom?

2. Material and methods

2.1. Study area

The study area was the northern sector of the North Atlantic from Greenland at 67°N, 46°W to Iceland at 67°N, 18°W, the Grand Banks at 50°N, 46°W to the MAR at 50°N, 18°W. In this area the RR is a prominent feature with a mean crest height of ~700 m below sea level and abyssal plains >3500 m deep on either side (Fig. 1A). At 52°N, the RR is segregated from the rest of the MAR by the Charlie-Gibbs Fracture Zone (CGFZ), where the North Atlantic Current (NAC) crosses the MAR, which results in an SST front (Fig. 1B). To test our hypothesis, four

* Corresponding author.
E-mail address: ghti@pml.ac.uk (G.H. Tilstone).

0034-4257/$ – see front matter.
http://dx.doi.org/10.1016/j.rse.2013.04.021

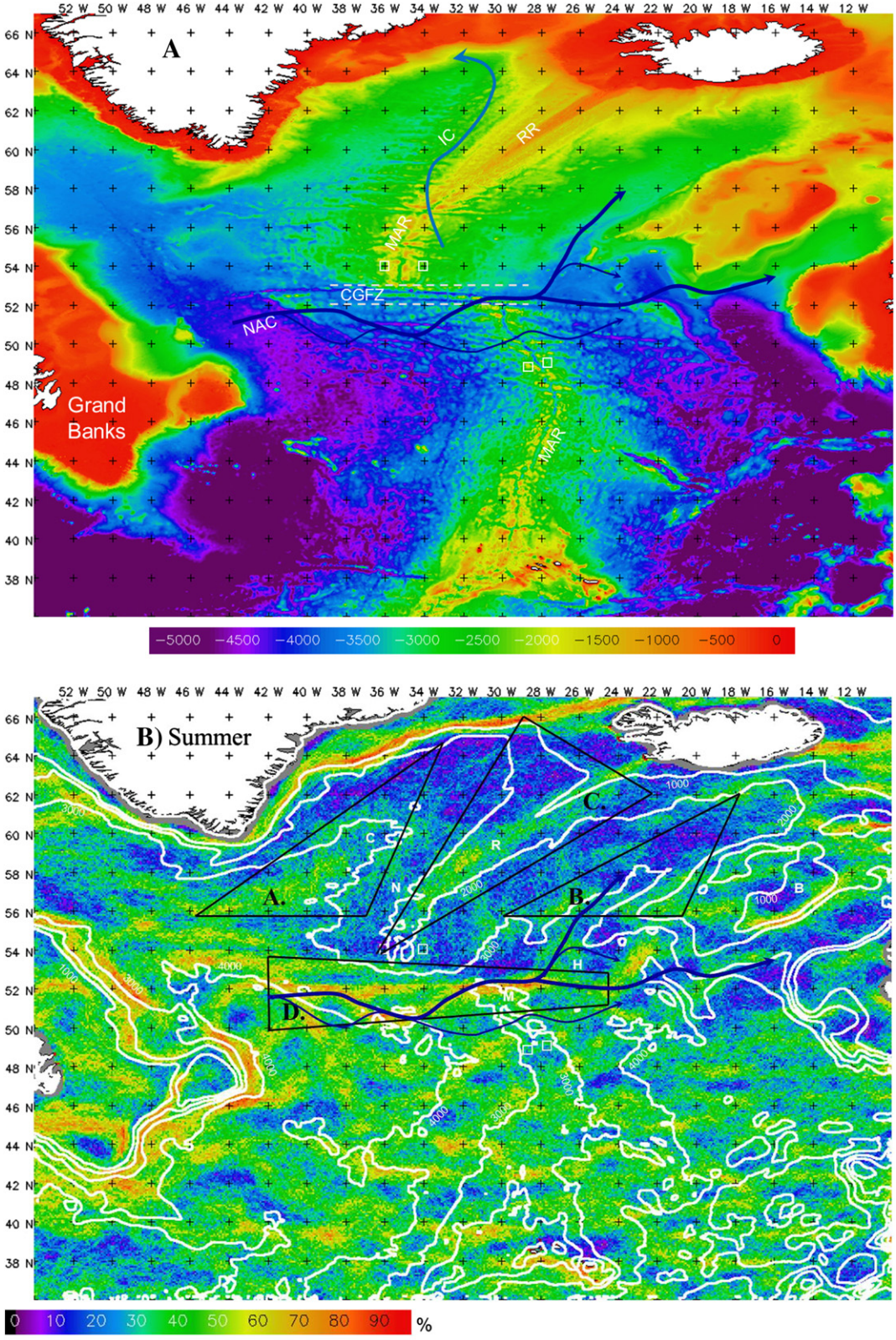

Fig. 1. (A.) Bathymetry of North Atlantic showing prominent ridges and mounts. West–east transverse arrow is the trajectory of the North Atlantic Current (NAC); thickness of the arrow represents the strength of the current. South–north arrow is the Irminger current (IC). RR = Reykjanes Ridge, MAR = Mid Atlantic Ridge, CGFZ = Charlie Gibbs Fracture Zone. White squares indicate the locations of ECOMAR moorings. (B.) Seasonal oceanic front frequency map for June to August, indicating the percentage of time a strong front was observed in merged microwave and infrared sea surface temperature data from 2006 to 2011. White contours are bathymetry. Black shapes represent areas from which the ocean colour data were extracted; A.) Central Irminger Sea, B.) Iceland Basin, C.) Reykjanes Ridge, D.) sub-polar front.

areas were identified using bathymetry and SST fronts as follows; open ocean waters of the a.) Central Irminger Sea (CIS), b.) Iceland Basin (ICB), c.) Reykjanes Ridge (RR) and d.) sub-polar front (SPF).

2.2. Remote sensing data

2.2.1. Thermal fronts

8-day composite front maps (Miller, 2009) were derived from daily merged microwave and infrared SST data for June to August from 2006 to 2011, and then aggregated to indicate regions where strong fronts are most frequently observed (Fig. 1B). The aggregation algorithm estimates the percentage of time a strong front is observed within each grid location (Miller, Read, & Dale, 2013).

2.2.2. Primary and new production

A wavelength resolving PP model (Morel, 1991) was implemented following Smyth, Tilstone, and Groom (2005) using the mean monthly 9 km NASA SeaWiFS OC4v4 Chla and Pathfinder v2009 AVHRR SST data to generate mean monthly satellite maps of PP from 1997 to 2010. The maximum quantum yield for growth (ϕ_m) and the maximum phytoplankton Chla-specific absorption coefficient (a^*_{max}) were parameterized using Chla following Morel, Antoine, Babin, and Dandonneau (1996). The model was forced with monthly satellite fields of Chla, SST and PAR (Frouin & Pinker, 1995). The PAR monthly fields are average daily integrated values. Downwelling irradiance values at each wavelength $E_d(\lambda)$ were retrieved using the look up table described in Smyth et al. (2005). Integration was performed over all daylight hours, from 400 to 700 nm, to the 1% light level and computed through the iterative approach of Morel and Berthon (1989). The model was run using surface Chla and temperature assuming a homogenous water column profile of Chla, a^*_{max} and ϕ_m. The estimates of satellite PP are accurate to 20% in the Atlantic Ocean (Tilstone, Smyth, Poulton, & Hutson, 2009).

New (=export) production (ExP) was calculated using the model of Laws, Falkowski, Smith, Ducklow, and McCarthy (2000), which converts surface PP to integrated ExP using a look table of export (ef) ratios derived from SST and net photosynthesis (mg N m^{-3} d^{-1}). The look up table was downloaded from the JGOFS web site and implemented in C^{++} to derive ef ratios from satellite values of AVHRR SST and surface net photosynthesis from the PP model. The model accounts for 86% of the variability in ef ratios derived from ^{15}N and ^{14}C uptake measurements and when primary production is <70 mmol C m^{-2} d^{-1} the model is accurate to 10–20% (Laws, 2004).

The spring bloom, defined as April to June based on Henson et al. (2009) and peak in PP climatology (Fig. 2), was masked out of the satellite data so that the effects of the ridge and front outside of the spring, could be assessed.

2.2.3. Phytoplankton community structure

The three-component phytoplankton biomass model of Brewin et al. (2010) was used to estimate micro-, nano- and pico-phytoplankton biomass using SeaWiFS data to investigate trends in community structure. The algorithm has been validated using 608 global satellite match-ups and the fraction of the three match-ups is accurate to 9.2% for micro-phytoplankton, 17.1% for nano-phytoplankton and 16.1% for pico-phytoplankton (Brewin, 2011).

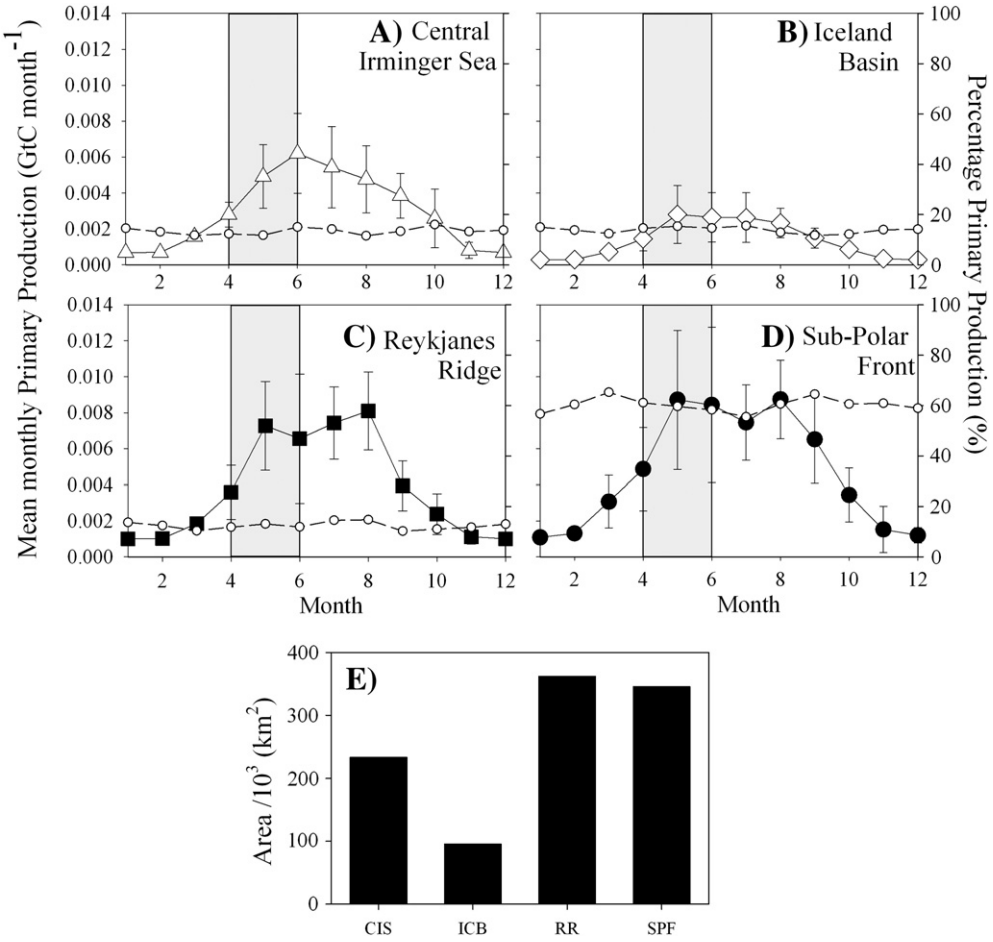

Fig. 2. Primary production climatology derived from 13 years of SeaWiFS data for (A.) Central Irminger Sea, (B.) Iceland Basin, (C.) Reykjanes Ridge, (D.) sub-polar front. Grey area represents the period of spring bloom, which was excluded from subsequent analyses. Dashed line and open circles in each plot are percentage monthly primary production based on the four areas from 13 years of SeaWiFS data and normalised by area. The area of each region (km^2) is given in (E.).

2.3. Statistical analyses

One way analysis of variance (ANOVA) was employed to assess differences between geographic areas. Kolomogrov–Smirnov with Lilliefors tests were used to check whether the distribution of in situ and satellite PP was normal, which were log transformed until no significant difference was found between the expected and the observed distributions. The results are given as $F_{3,579} = x$, $P = y$ where F is the mean square to mean square error ratio, the sub-script numbers denote the degrees of freedom (3) and number of samples (579). P is the ANOVA critical significance value. For the satellite time series of total Chla, micro-, nano-, pico-Chla and PP, anomalies were calculated by subtracting from each monthly value the corresponding monthly average for the time series from 1998 to 2010. Linear regression was fitted to the anomalies to assess inter-annual trends and Pearson correlation coefficients (r) and levels of significance (P) were used to evaluate significant trends. The cumulative sum method was applied to the anomalies to further decompose the signal to highlight major changes in monthly mean Chla values along the time-series (McQuatters-Gollop, Mee, Raitsos, & Shapiro, 2008).

3. Results

Analysis of SST data showed a strong and persistent front along the northern branch of the NAC (Fig. 1B) where it passes through the CGFZ (Fig. 1A) and delineates the SPF (Miller et al., in press). There was also a persistent front to the south-east of the SPF, close to the Grand Banks. Over the RR there was evidence of a persistent but weaker front running SW to NE, just west of the ridge. In the CIS, there was a weak front running NE to SW, whereas in the ICB there were no prominent fronts (Fig. 1B). A 13 year SeaWiFS climatology of PP (Fig. 2A–D) showed that outside of the spring bloom, there was a significantly higher PP over the SPF (0.021 GtC) and RR (0.018 GtC), which accounted for 14.8% and 8.6% of the North Atlantic PP respectively, compared to the ICB (0.005 GtC; 2.4%) and CIS (0.012 GtC; 6.9%) ($F_{3,579}$, $P < 0.0001$). For the RR and SPF a clear bi-modal peak in the mean monthly PP was observed, whereas for the CIS and ICB there was a single peak during the spring bloom only. When the monthly PP for each zone was normalised to area (Fig. 2E) and calculated as a percentage of the total of the four areas, the SPF was 4 times higher than the other zones (Fig. 2A–D). From July–September 1998–2010, PP was higher over both the RR and SPF compared with the CIS and ICB (Fig. 3). Analysis of the spatial homogeneity of the temporal patterns in these areas during summer is given in Fig. 4. PP over the CIS during July–September was the lowest of all regions and relatively homogenous from 35 to 45.5°W, except in 2007 and 2010 when there were notable increases (Fig. 4A). PP at the ICB was also low, but more heterogeneous, with higher values in 1999, 2000, 2004, 2005 and 2009 (Fig. 4B). PP over the RR from 27 to 33°W was comparatively higher except during 2004 and 2006 (Fig. 4C). For the SPF, PP from 23 to 43°W was consistently higher and at least double that of the CIS and ICB, especially during 1998–2001, 2006–2007 and 2009–2010 (Fig. 4D).

The annual ExP for these regions was ~50 g C m^{-2} yr^{-1} (Fig. 5A). During July–September ExP varied between 6 and 15 g C m^{-2} yr^{-1}, with the lowest in the ICB and consistently higher values at the SPF except in 2005 and 2006 (Fig. 5B). From 13 years of SeaWiFS data, Chla and PP increased significantly at the RR and CIS, which were associated with significant increases in micro- and nano-phytoplankton biomass (Fig. 6). These trends were forced by high values in summer 2010, which if removed from the time series, the relationships were no longer significant (Table 1). For the ICB, there was a significant increase in PP at the 5% significance level, but similarly if the 2010 were removed, there was no significant trend. There was no significant change in Chla, PP or size fractionated biomass at the SPF including or excluding the

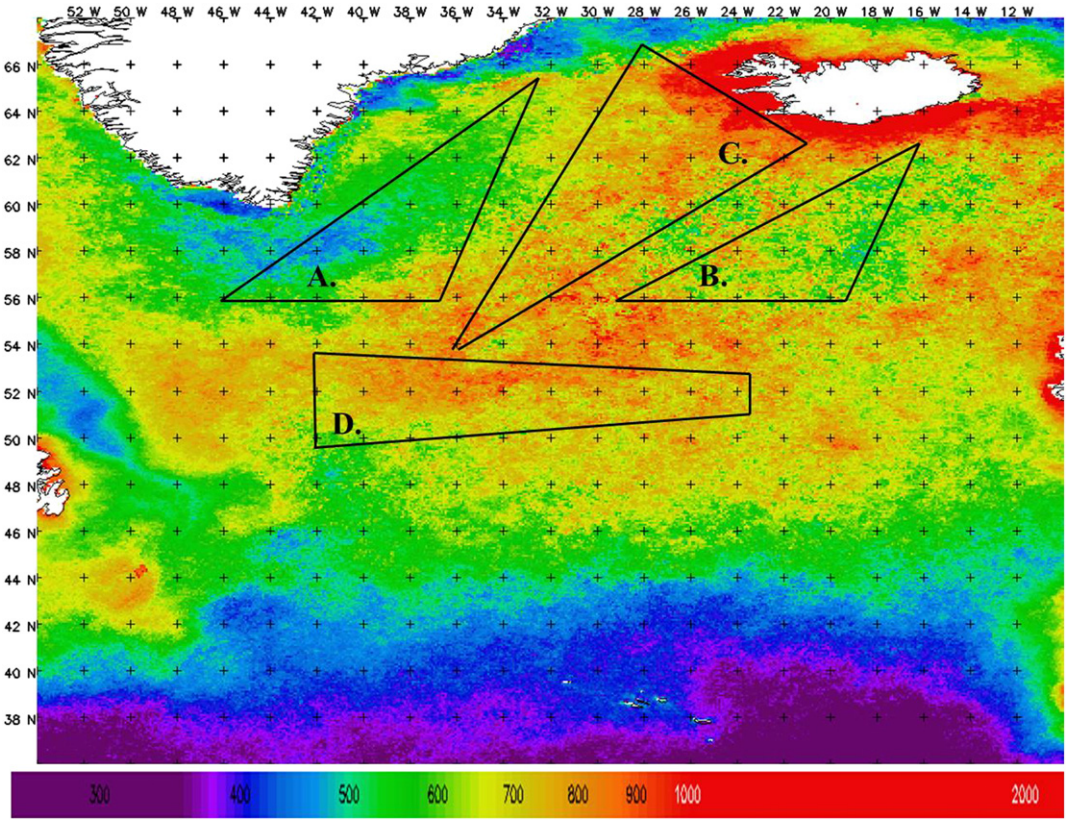

Fig. 3. Median primary production (mg C m^{-2} d^{-1}) for SeaWiFS July–September from 1998 to 2010. Areas as in Fig. 1B.

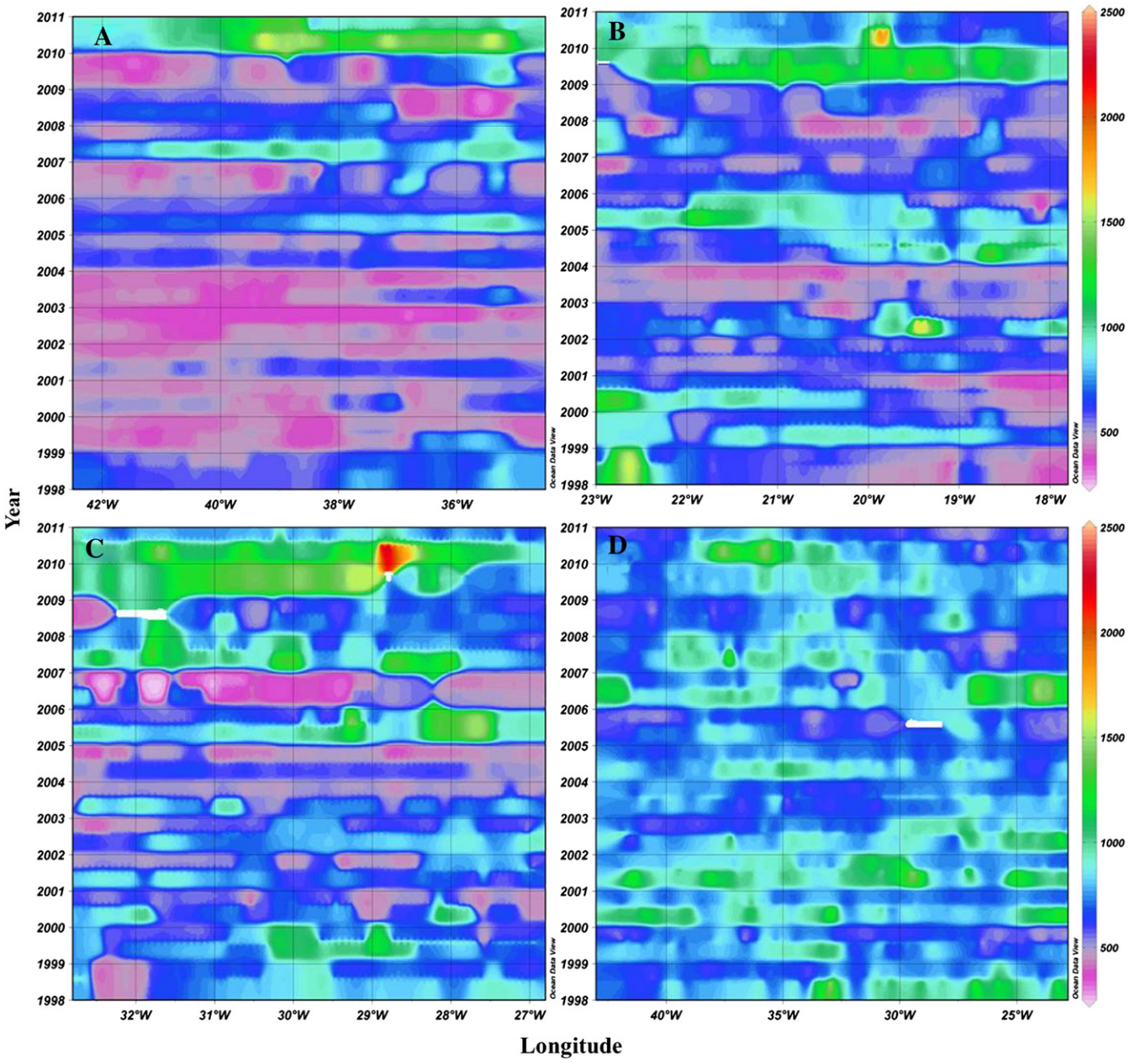

Fig. 4. Variability in primary production (mg C m^{-2} d^{-1}) during July–September from 1998 to 2010 along longitudinal transects in (A.) Central Irminger Sea at 59°N from 35 to 42°W, (B.) Iceland Basin at 59°N from 18 to 23°W, (C.) Reykjanes Ridge at 59°N from 27 to 33°W, (D.) sub-polar front at 52°N from 23 to 42°W.

2010 data (Fig. 6, Table 1), illustrating that in this region, there is a consistently higher and constant Chla, PP and ExP.

A comparison of monthly Chla anomalies from the Ocean Colour sensors SeaWiFS, MODIS and MERIS for each area and the combined North Atlantic area is given in Fig. 7. The associated correlation coefficients for the anomalies and levels of significance are given in Table 1. Similar to the trends shown in Fig. 6, MODIS and MERIS showed a significant increase in monthly Chla anomaly for the CIS, ICB, RR and North Atlantic from 2002 to 2010, but no significant change in Chla anomaly for the SPF over this period. If the 2010 data were not considered, there was still a significant increase in the Chla anomaly for the ICB, RR and the combined North Atlantic area, but there was no increase in the CIS and SPF (Table 1). Analysis of the cumulative sums in Chla, highlighted that for these areas there was no increase in SeaWiFS Chla from 1998 to 2002, except in the ICB which rose by 2 mg m^{-3} (Fig. 8A). From 2002 to 2007, Chla decreased in all areas and was most pronounced at the RR, where it decreased by ~5.5 mg m^{-3}. Chla then increased again to 2010, which was most prominent in the RR. MODIS and MERIS showed similar patterns with a decrease in Chla from 2002 to 2010 for all regions except the SPF (Fig. 8B, C). The CIS and ICB had a similar pattern to the combined North Atlantic area.

The variation in SeaWiFS Chla and PP in the CIS and ICB was driven by the North Atlantic Oscillation (NAO) with low NAO resulting in higher PP (Table 2). By contrast, there was no significant correlation between the NAO and PP at the RR and SPF, suggesting that these areas are less affected by the fluctuations in the NAO and, outside of the spring bloom, the greater frequency of fronts in summer (Fig. 1B) supports the higher PP (Fig. 3). Comparatively, PP at the RR was more variable than the SPF (Fig. 4, 8).

4. Discussion

From 44°W, saline Atlantic waters flow west–east as the Gulf Stream, which extends as the NAC at 40°W, is directed to the eastern

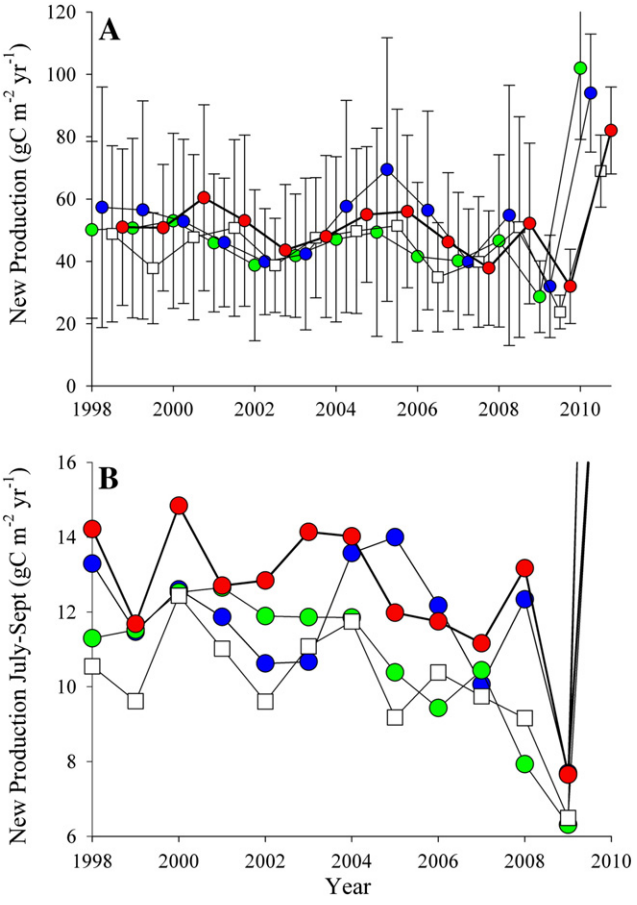

Fig. 5. (A.) Annual new production and (B.) new production excluding April to June from 1998 to 2010 for Central Irminger Sea (blue circle), Iceland Basin (open squares), Reykjanes Ridge (green circle), sub-polar front (red circles, solid line).

Atlantic basin through the transverse CGFZ (Bower & von Appen, 2008). Consequently a persistent east–west thermal front is formed at the edge of the NAC between 50 and 54°N (Fig. 1B), as surface water sinks through the deepest point of the CGFZ (Bower & von Appen, 2008). This marks the transition zone between East North Atlantic sub-tropical water and Arctic over-flow water (Pollard, Read, Holliday, & Leach, 2004). Close to the Grand Banks between 50 and 46°W, the SPF has been shown to trigger phytoplankton blooms through periodic stratification at the front (Taylor & Ferrari, 2011). The MAR can cause upwelling generated from crossing and tidal currents (Opdal, Godo, Bergstad, & Fiksen, 2008), which bring nutrient-rich water or autochthonous recycled nutrients to the surface (Mohn & Beckmann, 2002). Annual production for the North Atlantic is estimated to be 238 ± 22 g C m^{-2} yr^{-1} (Zhai et al., 2012). From our analysis between 66°N 46°W and 50°N 16°W, annual production for the SPF, RR, ICB, and CIS was 253 ± 20, 221 ± 40, 204 ± 33, and 184 ± 38 g C m^{-2} yr^{-1}, respectively. The spring bloom accounted for 57% of the PP. The SPF proved to be almost as productive (0.038 Gt C yr^{-1} including the spring bloom) as the California upwelling current (0.049 Gt yr^{-1}) (Carr, 2002). From continuous measurements of ^{17}O over the region, Quay, Stutsman, and Steinhoff (2012) suggested that high rates of production in the spring also continue through the summer, but the mechanism for this has not been identified. Outside of the spring bloom, we found that high PP occurred at the thermal fronts of the SPF and RR (Fig. 2D, 4A), which were 15 and 9% of the total for the North Atlantic. When normalised to area, PP over the SPF was four times higher than the RR (Fig. 2C, D). This could be due to the enhancement of nutrients in the photic zone of the front by turbulence-restratification events as described by Taylor and Ferrari (2011) or to the dilution-recoupling phenomena posed by Behrenfeld (2010). Further investigation of the nutrient dynamics and under-water light regime, that support PP across the SPF and RR during summer is necessary to elucidate the causes of enhanced PP in these regions outside of the spring bloom.

ExP can vary with time and is reported to be 50–80% of PP during episodic blooms or in high productivity areas, but much lower (5–10%) outside of these periods due to recycling and re-mineralisation of organic matter in the photic zone (Ganachaud & Wunsch, 2002). Different methods and models of ExP can vary by 60% (Henson et al., 2011). We therefore used new production as an indicator of potential export, which outside of the spring bloom illustrated that the SPF was 1.25 higher than the ICB and CIS (Fig. 5B). PP in these waters during late summer–autumn results in maximum CO_2 draw down (Takahashi et al., 2009) and very high carbon export efficiency (Levy et al., 2005). Our analysis suggests that the SPF potentially plays an important role in enhancing ExP in the North Atlantic and therefore in sustaining deep-sea biomass, which is affected more by annual production rates rather than the seasonality of the spring bloom (Letessier, Falkenhaug, Debes, Bergstad, & Brierley, 2011).

Recent studies in the North Atlantic have suggested that there has been a dramatic increase in the 'green-ness index' (PCI) of towed continuous plankton recorder (CPR) silks over the North Atlantic from 1995 to 2010 (McQuatters-Gollop et al., 2011). The CPR PCI reflects phytoplankton abundance and not biomass per se (Robinson, 1970), and can under-estimate Chla by a factor of 10–10^3 due to the large mesh size of the silks (Raitsos et al., 2013). A number of recent papers however, have shown that there is good agreement between PCI and SeaWiFS Chla, and that the under-estimate in PCI is constant due to consistent methods, so that the trends in PCI are representative for large areas (Batten, Walne, Edwards, & Groom, 2003; Raitsos, Reid, Lavender, Edwards, & Richardson, 2005). For the SeaWiFS time series, we observed a significant increase in Chla and the biomass of micro- and nano-phytoplankton and PP in the CIS and RR, but no significant change at the ICB and SPF. For the CIS and RR, this was principally driven by high values during summer 2010 (Fig. 6), when the Icelandic volcano Eyjafjallajökull erupted, which are either caused by high phytoplankton biomass due to deposition of micro-nutrients into the surface ocean (Olgun et al., 2011) or errors in the satellite atmospheric correction associated with volcanic particles (Porter, Kono, & Nielsen, 2005). Lin et al. (2011) found that the eruption of the Anahatan Volcano in the sub-tropical North Pacific, caused bloom like patches in the MODIS-Aqua ocean colour record, which were caused by a combination of suspended volcanic ash and phytoplankton, with a 2 to 5 fold increase in Chla caused by nitrate, phosphate and iron enrichment. Similarly Mantas, Pereira, and Morais (2011) observed anomalies in MODIS-Aqua Chla data, 17 times higher than back ground, during the eruption of the Home Reef Volcano close to Tonga in the South-West Pacific. These high Chla values can also be due to an over-estimate in SeaWiFS water leaving radiance caused by aerosols in the volcano plume as observed during the Hawaiin volcano, which when using the SeaDAS atmospheric correction implements an incorrect aerosol model (Porter et al., 2005). The use of longer wavelengths in the atmospheric correction model may be required to solve this problem, though this is beyond the scope of this paper. Excluding the 2010 data, there was no significant increase in Chla, micro-, nano-phytoplankton biomass and PP in the CIS and RR (Table 1). We did however, observe that over shorter term trends in MODIS-Aqua and MERIS Chla from 2002 to 2009, there was a significant increase in the ICB, RR and the combined North Atlantic area, but no change in Chla over the CIS and SPF. The CIS had a consistently low PP during July–September from 1998 to 2011 (Fig. 3) and the PP in the SPF was consistently high, whereas PP in the ICB and RR was more heterogeneous (Fig. 4). Time series analyses over large areas can potentially obscure localised heterogeneous variations in Chla and PP caused by area specific variations in the physico-chemical

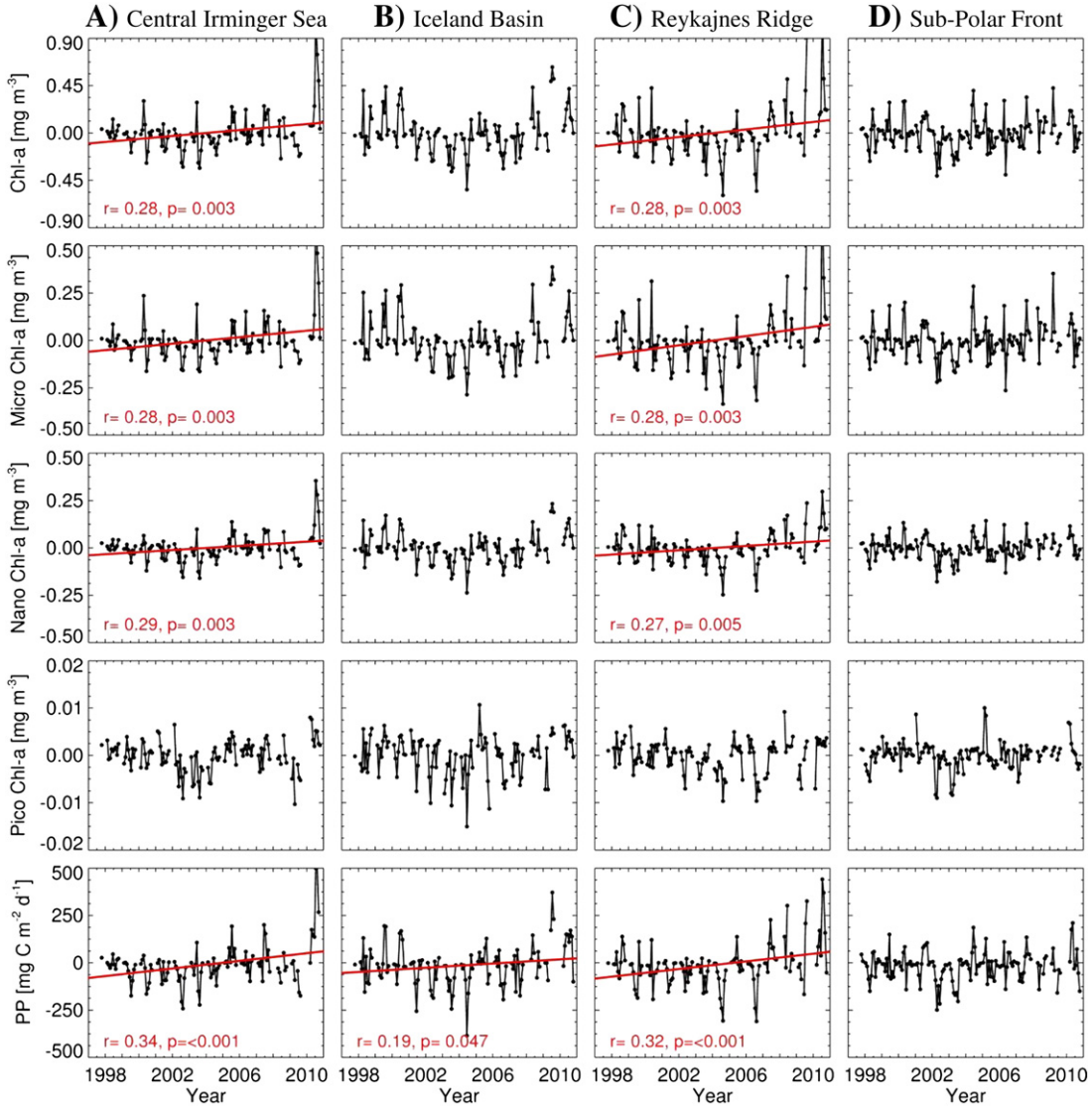

Fig. 6. Monthly SeaWiFS Chlorophyll-a anomaly (mg m^{-3}), of micro-, nano-, pico-phytoplankton, total Chla and primary production 'PP (mg C m^{-2} d^{-1}) for (A.) Central Irminger Sea, (B.) Iceland Basin, (C.) Reykjanes Ridge and (D.) sub-polar front.

environment. If the data for the North Atlantic is pooled over large areas, for example (McQuatters-Gollop et al., 2011), the fine scale spatial patterns that sustain high biomass and production at the SPF (Figs. 3, 4), become blurred. At the SPF, higher PP could be associated with a shift of the NAC into the Iceland Basin and a strengthening of the sub-polar gyre (Hakkinen & Rhines, 2004). This implies that a weakening of the sub-polar gyre leads to a reduction in PP and ExP over the SPF, which would potentially reduce carbon export to the benthos. For the RR, the persistent cold water, nutrient rich front on the western ridge (Mauritzen et al., 2002) (Fig. 1B) is associated with the trajectory of the NAC and Irminger currents as they flow northwards along the western slope (Sarafanov et al., 2010). Our analysis showed that the front on the western slope, sustains high biomass and productivity outside of the spring bloom, though there is considerable inter-annual variability during the summer months, presumably due to the strength and location of the NAC and Irminger currents.

Extreme fluctuations in atmospheric forcing of the sub-polar zone have occurred over the past 30 years and are reflected by the NAO (Hakkinen & Rhines, 2004). The NAC branches north-eastward close to the Rockall Trough (Orvik & Skagseth, 2003), and depending on the strength of the sub-polar gyre (Hatun, Sando, Drange, Hansen, & Valdimarsson, 2005), is topographically steered either into the Faroe–Shetland Channel or the Iceland basin (Hakkinen & Rhines, 2009). Positive NAO results in a later spring bloom in North Atlantic sub-polar waters (Henson et al., 2009). We found a significant negative relationship between NAO and PP in the CIS and ICB (Table 2). During the SeaWiFS time series from 1997 to 2000, there was an intense reversal of the winter NAO index which caused a decline in the sub-polar gyre surface currents (Hakkinen & Rhines, 2004) and resulted in an increase in Chla, micro-phytoplankton biomass and PP at the RR, SPF and ICB (Fig. 6). From 2001 to 2005 the NAO then fluctuated between weak positive and negative (Hakkinen & Rhines, 2009), which lead to a slow down and contraction of the sub-polar gyre (Sarafanov et al., 2010), which resulted in lower Chla and PP values associated with a negative micro-phytoplankton anomaly in all regions. After 2006, the NAO switched to positive with little effect on Chla and PP in all regions except the CIS, which increased by ~3 mg m^{-3} (Fig. 8). We found that fluctuations in the NAO had a significant effect on PP in the CIS and ICB, but did not significantly influence PP at the RR and SPF. This therefore suggests that

Table 1
Pearson correlation coefficients between anomalies of SeaWiFS size-fractionated Chla, primary production (PP), SeaWiFS, MODIS, and MERIS total chlorophyll-a (Chla) from 1998 to 2010 and 1998 to 2009 in different areas of the North Atlantic. Significant regressions are given in bold.

Area	Linear regression of anomalies over time (1998–2010)		Linear regression of Chla anomaly over time (1998–2009)	
	Correlation coefficient (r)	P-value	Correlation coefficient (r)	P-value
PP				
A. Central Irminger Sea	**0.34**	<**0.001**	0.09	0.364
B. Iceland Basin	**0.19**	**0.047**	0.08	0.430
C. Reykajnes Ridge	**0.32**	<**0.001**	0.18	0.069
D. Sub-polar front	0.07	0.407	0.01	0.912
Micro-Chla				
A. Central Irminger Sea	**0.28**	**0.003**	0.04	0.673
B. Iceland Basin	0.09	0.370	−0.01	0.912
C. Reykajnes Ridge	**0.28**	**0.003**	0.16	0.105
D. Sub-polar front	0.10	0.233	0.09	0.326
Nano-Chla				
A. Central Irminger Sea	**0.29**	**0.003**	0.03	0.727
B. Iceland Basin	0.10	0.277	−0.03	0.798
C. Reykajnes Ridge	**0.27**	**0.005**	0.10	0.314
D. Sub-polar front	0.06	0.494	0.02	0.843
Pico-Chla				
A. Central Irminger Sea	0.07	0.447	−0.14	0.166
B. Iceland Basin	0.02	0.858	0.12	0.240
C. Reykajnes Ridge	−0.02	0.867	−0.12	0.207
D. Sub-polar front	0.07	0.407	0.01	0.912
Total Chla SeaWiFS				
A. Central Irminger Sea	**0.28**	**0.003**	0.04	0.721
B. Iceland Basin	0.09	0.329	−0.02	0.846
C. Reykajnes Ridge	**0.28**	**0.003**	0.14	0.164
D. Sub-polar front	0.09	0.304	0.06	0.485
E. All North Atlantic regions	**0.29**	<**0.001**	0.08	0.400
Total Chla MODIS-aqua (2002–2010)				
A. Central Irminger Sea	**0.42**	<**0.001**	0.17	0.173
B. Iceland Basin	**0.44**	<**0.001**	**0.31**	**0.011**
C. Reykajnes Ridge	**0.48**	<**0.001**	**0.40**	<**0.001**
D. Sub-polar front	0.01	0.915	0.07	0.503
E. All North Atlantic regions	**0.49**	<**0.001**	**0.33**	**0.003**
Total Chla MERIS (2002–2010)				
A. Central Irminger Sea	**0.40**	<**0.001**	0.12	0.323
B. Iceland Basin	**0.45**	<**0.001**	**0.36**	**0.003**
C. Reykajnes Ridge	**0.37**	**0.002**	**0.47**	<**0.001**
D. Sub-polar front	0.03	0.772	0.11	0.303
E. All North Atlantic regions	**0.47**	<**0.001**	**0.31**	**0.004**

the SPF and to a lesser extent the RR, always sustain a higher and persistent Chla biomass and PP due to the associated thermal front, irrespective of climatic oscillations.

5. Conclusions

Analysis of 13 years of multiple satellite data showed persistent thermal signatures at the RR and SPF, which sustained high PP outside of the spring bloom, accounting for 9 and 15% of the PP in the North Atlantic. SeaWiFS, MODIS-Aqua and MERIS ocean colour records, showed that there was no change in Chla from 1998 to 2002, followed by a decrease in Chla from 2002 to 2007, which then increased from 2008 to 2010. The SPF exhibited the highest PP and the lowest variation in Chla. This implies that the SPF sustains high export production in the North Atlantic, and is less affected by fluctuations in the North Atlantic Oscillation compared to other areas.

Acknowledgements

Ocean colour imagery was supplied by the Natural Environment Research Council (NERC) Earth Observation Data Acquisition and Analysis Service (NEODAAS) at Plymouth Marine Laboratory. Merged microwave and infrared SST data were provided by Remote Sensing Systems. Thanks to Christina Houlgreave for processing Fig. 3 and Ocean Data View software to enable us to produce Fig. 4. IGP and PIM were supported by the NERC-UK ECOMAR (NE/C513018/1), RJWB by NERC-UK NCEO and ESA OC-CCI and GHT by the NERC-UK Ocean 2025 research programme.

References

Batten, S. D., Walne, A. W., Edwards, M., & Groom, S. B. (2003). Phytoplankton biomass from continuous plankton recorder data: An assessment of the phytoplankton colour index. *Journal of Plankton Research*, *25*, 697–702.
Behrenfeld, M. J. (2010). Abandoning Sverdrup's Critical Depth Hypothesis on phytoplankton blooms. *Ecology*, *91*, 977–989.
Bower, A. S., & von Appen, W. -J. (2008). Interannual variability in the pathways of the North Atlantic current over the Mid-Atlantic Ridge and the impact of topography. *Journal of Physical Oceanography*, *38*, 104–120.
Brewin, R. J. W. (2011). Detecting phytoplankton size class using Earth Observation. *Institute of Marine Science*. Plymouth: University of Plymouth.
Brewin, R. J. W., Sathyendranath, S., Hirata, T., Lavender, S. J., Barciela, R. M., & Hardman-Mountford, N. J. (2010). A three-component model of phytoplankton size class for the Atlantic Ocean. *Ecological Modelling*, *221*, 1472–1483.
Carr, M. E. (2002). Estimation of potential productivity in Eastern Boundary Currents using remote sensing. *Deep Sea Research Part II—Topical Studies in Oceanography*, *49*, 59–80.
Dutkiewicz, S., Follows, M., Marshall, J., & Gregg, W. W. (2001). Interannual variability of phytoplankton abundances in the North Atlantic. *Deep Sea Research Part II—Topical Studies in Oceanography*, *48*, 2323–2344.
Frouin, R., & Pinker, R. T. (1995). Estimating photosynthetically active radiation (Par) at the Earths surface from satellite-observations. *Remote Sensing of Environment*, *51*, 98–107.
Ganachaud, A., & Wunsch, C. (2002). Oceanic nutrient and oxygen transports and bounds on export production during the World Ocean Circulation Experiment. *Global Biogeochemical Cycles*, *16*.
Hakkinen, S., & Rhines, P. B. (2004). Decline of subpolar North Atlantic circulation during the 1990s. *Science*, *304*, 555–559.
Hakkinen, S., & Rhines, P. B. (2009). Shifting surface currents in the northern North Atlantic Ocean. *Journal of Geophysical Research-Oceans*, *114*.
Hatun, H., Sando, A.B., Drange, H., Hansen, B., & Valdimarsson, H. (2005). Influence of the Atlantic subpolar gyre on the thermohaline circulation. *Science*, *309*, 1841–1844.
Henson, S. A., Dunne, J. P., & Sarmiento, J. L. (2009). Decadal variability in North Atlantic phytoplankton blooms. *Journal of Geophysical Research-Oceans*, *114*.
Henson, S. A., Sanders, R., Madsen, E., Morris, P. J., Le Moigne, F., & Quartly, G. D. (2011). A reduced estimate of the strength of the ocean's biological carbon pump. *Geophysical Research Letters*, *38*.
Hitchcock, G. L., Langdon, C., & Smayda, T. J. (1987). Short-term changes in the biology of a Gulf-Stream warm-core ring — Phytoplankton biomass and productivity. *Limnology and Oceanography*, *32*, 919–928.
Koertzinger, A., Send, U., Lampitt, R. S., Hartman, S., Wallace, D. W. R., Karstensen, J., et al. (2008). The seasonal pCO(2) cycle at 49 degrees N/16.5 degrees W in the northeastern Atlantic Ocean and what it tells us about biological productivity. *Journal of Geophysical Research—Oceans*, *113*.
Laws, E. A. (2004). New production in the equatorial Pacific: A comparison of field data with estimates derived from empirical and theoretical models. *Deep Sea Research Part I—Oceanographic Research Papers*, *51*, 205–211.
Laws, E. A., Falkowski, P. G., Smith, W. O., Ducklow, H., & McCarthy, J. J. (2000). Temperature effects on export production in the open ocean. *Global Biogeochemical Cycles*, *14*, 1231–1246.
Letessier, T. B., Falkenhaug, T., Debes, H., Bergstad, O. A., & Brierley, A. S. (2011). Abundance patterns and species assemblages of euphausiids associated with the Mid-Atlantic Ridge, North Atlantic. *Journal of Plankton Research*, *33*, 1510–1525.
Levy, M., Lehahn, Y., Andre, J. M., Memery, L., Loisel, H., & Heifetz, E. (2005). Production regimes in the northeast Atlantic: A study based on Sea-viewing Wide Field-of-view Sensor (SeaWiFS) chlorophyll and ocean general circulation model mixed layer depth. *Journal of Geophysical Research—Oceans*, *110*.
Lin, I. I., Hu, C., Li, Y. -H., Ho, T. -Y., Fischer, T. P., Wong, G. T. F., et al. (2011). Fertilization potential of volcanic dust in the low-nutrient low-chlorophyll western North Pacific subtropical gyre: Satellite evidence and laboratory study. *Global Biogeochemical Cycles*, *25*.
Longhurst, A., Sathyendranath, S., Platt, T., & Caverhill, C. (1995). An estimate of global primary production in the ocean from satellite radiometer data. *Journal of Plankton Research*, *17*, 1245–1271.
Mantas, V. M., Pereira, A. J. S.C., & Morais, P. V. (2011). Plumes of discolored water of volcanic origin and possible implications for algal communities. The case of the Home Reef eruption of 2006 (Tonga, Southwest Pacific Ocean). *Remote Sensing of Environment*, *115*, 1341–1352.
Mauritzen, C., Polzin, K. L., McCartney, M. S., Millard, R. C., & West-Mack, D. E. (2002). Evidence in hydrography and density fine structure for enhanced vertical mixing

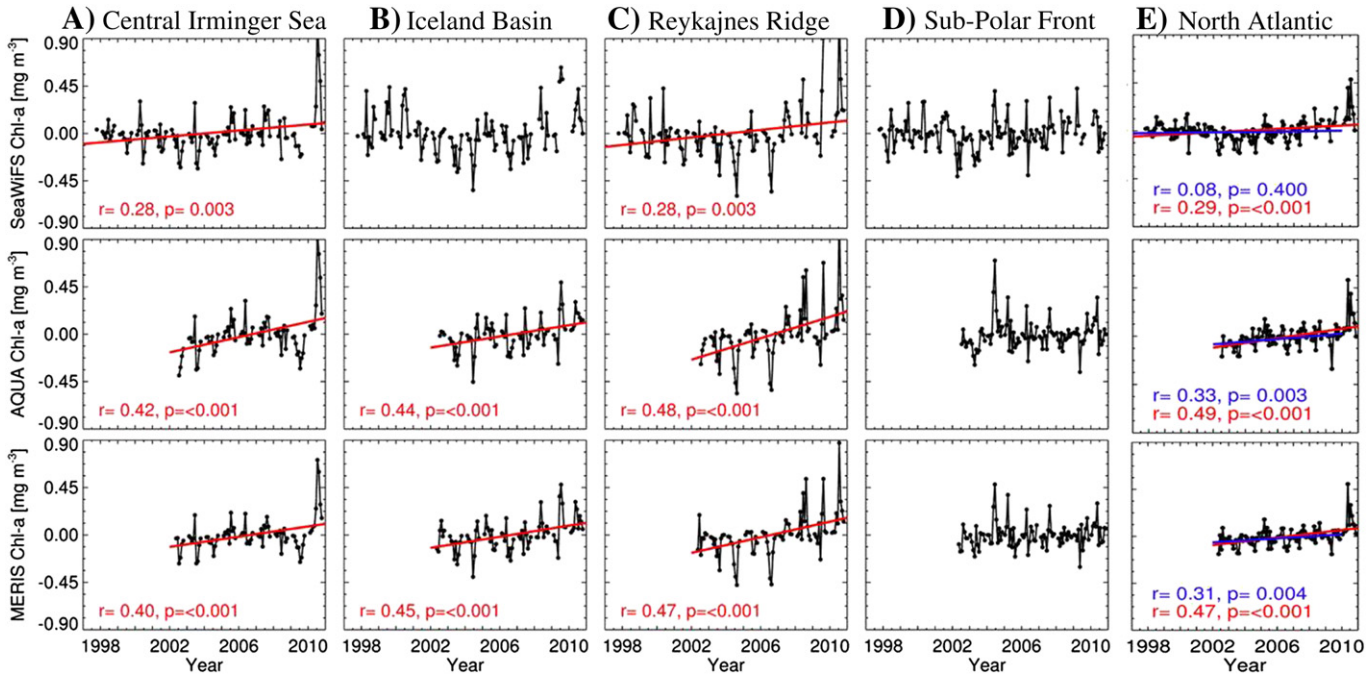

Fig. 7. Monthly Total Chlorophyll-a anomaly (mg m^{-3}) with Pearson correlation coefficient and significance level from 1998 to 2010 for SeaWiFS, MODIS-Aqua and MERIS for (A.) Central Irminger Sea, (B.) Iceland Basin, (C.) Reykjanes Ridge, (D.) sub-polar front and (E.) combined North Atlantic area. In (E.) Pearson correlation coefficient and significance level given in blue is for the period 1998 to 2009.

over the Mid-Atlantic Ridge in the western Atlantic. *Journal of Geophysical Research—Oceans*, *107*.

McQuatters-Gollop, A., Mee, L. D., Raitsos, D. E., & Shapiro, G. I. (2008). Non-linearities, regime shifts and recovery: The recent influence of climate on Black Sea chlorophyll. *Journal of Marine Systems*, *74*, 649–658.

McQuatters-Gollop, A., Reid, P. C., Edwards, M., Burkill, P. H., Castellani, C., Batten, S., et al. (2011). Is there a decline in marine phytoplankton? *Nature*, *472*, E6–E7.

Miller, P. (2009). Composite front maps for improved visibility of dynamic sea-surface features on cloudy SeaWiFS and AVHRR data. *Journal of Marine Systems*, *78*, 327–336.

Miller, P. I., Read, J. F., & Dale, A. C. (2013). Thermal front variability along the North Atlantic Current observed using satellite microwave and infrared data. *Deep Sea Research Part II: Topical Studies in Oceanography*, http://dx.doi.org/10.1016/j.dsr2.2013.08.014 (in press).

Mohn, C., & Beckmann, A. (2002). Numerical studies on flow amplification at an isolated shelfbreak bank, with application to Porcupine Bank. *Continental Shelf Research*, *22*, 1325–1338.

Morel, A. (1991). Light and marine photosynthesis — A spectral model with geochemical and climatological implications. *Progress in Oceanography*, *26*, 263–306.

Morel, A., Antoine, D., Babin, M., & Dandonneau, Y. (1996). Measured and modeled primary production in the northeast Atlantic (EUMELI JGOFS program): The impact of natural variations in photosynthetic parameters on model predictive skill. *Deep Sea Research Part I—Oceanographic Research Papers*, *43*, 1273–1304.

Morel, A., & Berthon, J. F. (1989). Surface pigments, algal biomass profiles, and potential production of the euphotic layer — Relationships reinvestigated in view of remote-sensing applications. *Limnology and Oceanography*, *34*, 1545–1562.

Olgun, N., Duggen, S., Croot, P. L., Delmelle, P., Dietze, H., Schacht, U., et al. (2011). Surface ocean iron fertilization: The role of airborne volcanic ash from subduction zone and hot spot volcanoes and related iron fluxes into the Pacific Ocean. *Global Biogeochemical Cycles*, *25*.

Opdal, A. F., Godo, O. R., Bergstad, O. A., & Fiksen, O. (2008). Distribution, identity, and possible processes sustaining meso- and bathypelagic scattering layers on the northern Mid-Atlantic Ridge. *Deep-Sea Research Part II—Topical Studies in Oceanography*, *55*, 45–58.

Orvik, K. A., & Skagseth, O. (2003). The impact of the wind stress curl in the North Atlantic on the Atlantic inflow to the Norwegian Sea toward the Arctic. *Geophysical Research Letters*, *30*.

Pingree, R., Kuo, Y. H., & Garcia-Soto, C. (2002). Can the Subtropical North Atlantic permanent thermocline be observed from space? *Journal of the Marine Biological Association of the United Kingdom*, *82*, 709–728.

Pollard, R. T., Read, J. F., Holliday, N.P., & Leach, H. (2004). Water masses and circulation pathways through the Iceland Basin during Vivaldi 1996. *Journal of Geophysical Research—Oceans*, *109*.

Porter, J., Kono, S., & Nielsen, T. (2005). Atmospheric correction errors under the Hawaii volcano: Possible solutions. In R. J. K. H. P. D. Frouin (Ed.), *Active and passive remote sensing of the oceans* (pp. 78–84).

Quay, P., Stutsman, J., & Steinhoff, T. (2012). Primary production and carbon export rates across the subpolar N. Atlantic Ocean basin based on triple oxygen isotope and dissolved O^{-2} and Ar gas measurements. *Global Biogeochemical Cycles*, *26*.

Raitsos, D. E., Reid, P. C., Lavender, S. J., Edwards, M., & Richardson, A. J. (2005). Extending the SeaWiFS chlorophyll data set back 50 years in the northeast Atlantic. *Geophysical Research Letters*, *32*.

Raitsos, D. E., Walne, A., Lavender, S. J., Licandro, P., Reid, P. C., & Edwards, M. (2013). A 60-year ocean colour data set from the continuous plankton recorder. *Journal of Plankton Research*, *35*, 158–164.

Robinson, G. A. (1970). Continuous plankton records: Variation in the seasonal cycle of phytoplankton in the North Atlantic. *Bulletin of Marine Ecology*, *6*, 333–345.

Sarafanov, A., Falina, A., Lherminier, P., Mercier, H., Sokov, A., & Gourcuff, C. (2010). Assessing decadal changes in the Deep Western Boundary Current absolute transport southeast of Cape Farewell, Greenland, from hydrography and altimetry. *Journal of Geophysical Research—Oceans*, *115*.

Smyth, T. J., Tilstone, G. H., & Groom, S. B. (2005). Integration of radiative transfer into satellite models of ocean primary production. *Journal of Geophysical Research—Oceans*, *110*.

Sverdrup, H. U. (1957). On conditions for the vernal blooming of phytoplankton. *Journal du Conseil International pour l'Exploration de la Mer*, *18*, 287–295.

Takahashi, T., Sutherland, S.C., Wanninkhof, R., Sweeney, C., Feely, R. A., Chipman, D. W., et al. (2009). Climatological mean and decadal change in surface ocean pCO(2), and net sea–air CO(2) flux over the global oceans (vol 56, pg 554, 2009). *Deep Sea Research Part I-Oceanographic Research Papers*, *56*, 2075–2076.

Taylor, J. R., & Ferrari, R. (2011). Ocean fronts trigger high latitude phytoplankton blooms. *Geophysical Research Letters*, *38*.

Tilstone, G., Smyth, T., Poulton, A., & Hutson, R. (2009). Measured and remotely sensed estimates of primary production in the Atlantic Ocean from 1998 to 2005. *Deep Sea Research Part II—Topical Studies in Oceanography*, *56*, 918–930.

Wassmann, P. (1990). Relationship between primary and export production in the boreal coastal zone of the North Atlantic. *Limnology and Oceanography*, *35*, 464–471.

Zhai, L., Gudmundsson, K., Miller, P., Peng, W., Gudfinnsson, H., Debes, H., et al. (2012). Phytoplankton phenology and production around Iceland and Faroes. *Continental Shelf Research*, *37*, 15–25.

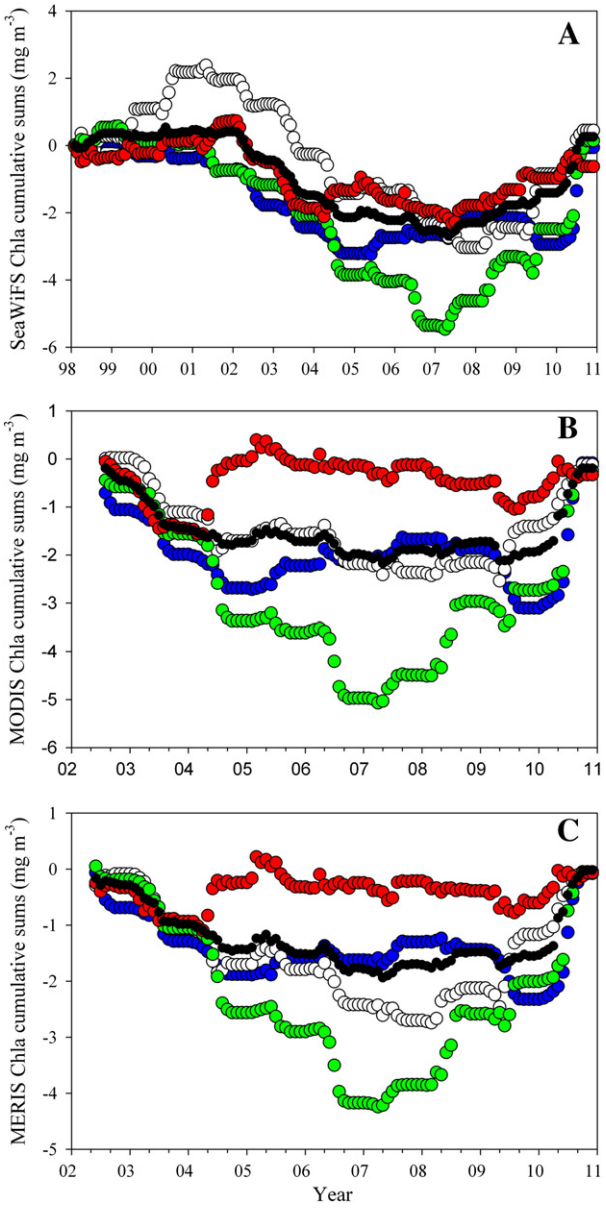

Fig. 8. Cumulative sums for Total Chlorophyll-a (mg m^{-3}) from (A.) SeaWiFS, (B.) MODIS-aqua, (C.) MERIS for Central Irminger Sea (blue circles), Iceland Basin (white, open circles), Reykjanes Ridge (green circles), sub-polar front and (red circles) combined North Atlantic area (black circles).

Table 2
Pearson correlation between North Atlantic Oscillation (NAO) and primary production (PP) for different areas of the North Atlantic Ocean for the period 1998–2010. Significant regressions are given in bold.

Area	NAO versus PP	
	Correlation coefficient (r)	P-value
A. Central Irminger Sea	**−0.196**	**0.040**
B. Iceland Basin	**−0.277**	**0.003**
C. Reykajnes Ridge	−0.160	0.091
D. Sub-polar front	−0.099	0.254